Special Feature: Energy Conversion and Storage

Research Report

Electrochemical Performance of an All-solid-state Lithium Ion Battery Using Garnet-type Oxide Electrolytes

Shingo Ohta, Tetsuro Kobayashi and Takahiko Asaoka

Report received on Aug. 30, 2013

ABSTRACT All-solid-state lithium ion batteries containing solid electrolytes are considered to be safer than lithium ion batteries that use liquid organic electrolytes. Therefore, new solid electrolytes are strongly required to improve the performance of all-solid-state lithium ion batteries. The lithium garnet-type oxide $Li_7La_3Zr_2O_{12}$ is expected to be a promising candidate as a solid electrolyte because it has advantages such as high chemical stability and a wide potential window. However, the lithium ion conductivity of $Li_7La_3Zr_2O_{12}$ is ~0.2 mS cm^{-1} at 25 °C, which is approximately two orders of magnitude lower than that of conventional liquid organic electrolytes. In this study, the lithium ion conductivity of $Li_7La_3Zr_2O_{12}$ was successfully improved by Nb-doping and optimization of the composition. The lithium ion conductivity of $Li_{7-X}La_3(Zr_{2-X}, Nb_X)O_{12}$ increased with the Nb content and reached a maximum of ~0.8 mS cm^{-1} (25 °C) at around X = 0.25, which is comparable to that of other fast lithium ion conducting oxides such as NASICON type oxides. An all-solid-state lithium ion battery was constructed using $Li_{6.75}La_3(Zr_{1.75}, Nb_{0.25})O_{12}$ (solid electrolyte), lithium (anode) and $LiCoO_2$ (cathode), and good charge and discharge characteristics were obtained. Therefore, it is concluded that $Li_{6.75}La_3(Zr_{1.75}, Nb_{0.25})O_{12}$ is a promising candidate as a solid electrolyte for all-solid-state lithium ion batteries.

KEYWORDS Garnet-type Oxide, Lithium Ion Conductor, All-solid-state Lithium Ion Battery, Solid Electrolyte, Ceramics, PLD

1. Introduction

All-solid-state lithium ion batteries with solid electrolytes are considered to be safer than lithium ion batteries that use liquid organic electrolytes due to their nonflammability. In addition, solid oxide electrolytes are believed to have a potential advantage over other inorganic materials in terms of their chemical stability, for example, they do not release toxic gases when decomposed. All-solid-state lithium ion batteries with solid oxide electrolytes have attracted significant attention due to these advantages.

In order to improve the performance of all-solid-state lithium ion secondary batteries, new solid electrolytes are required with the following properties: (1) a high lithium ionic conductivity, with a negligible electron contribution (conduction), (2) stability against chemical reaction with lithium at the anode, and Co-, Ni-, or Mn-containing oxides at the cathode, and (3) a wide electrochemical window allowing the use of high-voltage cathode materials (≥ 5 V vs. Li^+/Li) and lithium metal anodes. The glassy lithium phosphorus oxynitride (LiPON)[1] was proposed for use in a thin-film solid-state lithium ion battery, and was confirmed to function as a solid-state electrolyte.[2] However, the low power density of solid-state lithium ion batteries using LiPON was considered disadvantageous due to the low lithium ion conductivity of LiPON (~1 μS cm^{-1} at room temperature). Some oxide materials, such as perovskite-type oxides (Li, La)TiO_3[3,4] or NASICON-type structured oxides, e.g., $LiTi_2P_3O_{12}$,[5] and their derivatives,[6] exhibit high lithium ion conductivity (~1 mS cm^{-1} at room temperature) but are not yet applicable as electrolytes in lithium ion batteries because they allow lithium insertion to reduce Ti^{4+} to Ti^{3+} around 1.5 V vs. Li^+/Li. To date, no oxide material has been reported to have both high lithium ion conductivity and a wide electrochemical window.

2. Garnet-type Oxides

The lithium garnet-type oxides available for use as solid oxide electrolytes are represented by the chemical composition $Li_xA_3M_2O_{12}$ (A: rare earth metal or alkali earth metal, M: tetravalent or pentavalent metal, X = 5-7 (balance of charge compensation for the

cation and anion)). The lithium ion conductivity of $Li_5La_3Nb_2O_{12}$ and its derivatives,[7-11] which were examined within the last decade, was still low (~1 μS cm^{-1} at R.T.), but $Li_7La_3Zr_2O_{12}$ reported by Thangadurai and Weppner in 2007[12] shows high lithium ion conductivity (~0.1 mS cm^{-1} at R.T.) that is approximately two orders of magnitude higher than that of conventional lithium garnet-type oxides. Moreover, $Li_7La_3Zr_2O_{12}$ has high chemical stability and a wide potential window, and is thus, considered to be a promising candidate solid electrolyte. However, it is necessary to improve the lithium ion conductivity of $Li_7La_3Zr_2O_{12}$ to develop an all-solid-state lithium ion battery with good electrochemical performance. To improve the lithium ion conductivity of $Li_7La_3Zr_2O_{12}$, the composition was optimized by Nb-doping. As a result, the lithium ion conductivity of $Li_7La_3Zr_2O_{12}$ was successfully improved to a maximum conductivity of ~0.8 mS cm^{-1} at 25 °C.

3. Nb Substituted $Li_7La_3Zr_2O_{12}$

Nb substituted $Li_7La_3Zr_2O_{12}$ ($Li_{7-X}La_3(Zr_{2-X}, Nb_X)O_{12}$ (X = 0-2) was prepared by conventional solid-state reaction.[13] **Figure 1**(a) shows XRD patterns of the $Li_{7-X}La_3(Zr_{2-X}, Nb_X)O_{12}$ samples. All of the observed diffraction peaks were indexed as a cubic lithium garnet-like structure (space group: *Ia-3d*). Lattice parameters of the $Li_{7-X}La_3(Zr_{2-X}, Nb_X)O_{12}$ samples calculated from their XRD patterns are shown in Fig. 1(b). The Lattice parameter of $Li_{7-X}La_3(Zr_{2-X}, Nb_X)O_{12}$ decreased linearly with increasing Nb-content (X) according to Vegard's law, indicating that Nb^{5+} (86.0 pm) was substituted at Zr^{4+} (70.9 pm) sites.

The electrical conductivity of the samples was measured in air using a two-probe AC impedance method with an Agilent 4294A in the frequency range of 40 Hz to 110 MHz at temperatures from 25 to 150 °C. The density of all measurement samples was between 89 and 92% of the theoretical density calculated from the lattice parameters. **Figure 2** shows a Nyquist plot of $Li_{6.75}La_3(Zr_{1.75}, Nb_{0.25})O_{12}$ at 25 °C in air. The plot can be well-resolved into bulk, grain-boundry, and electrode resistances. The semicircle in the high-frequency region represents the bulk resistance, and the other one represents the grain-boundary resistance. The appearance of a tail at the low-frequency region suggests that the electrode blocked mobile lithium ions. The solid line in Fig. 2 represents fitted data based on an equivalent circuit model consisting of two parallel resistance (R) and capacitance (C) contributions $(R_bC_b)(R_{gb}C_{gb})(R_{el})$, where b, gb, and el denote the bulk, grain-boundary, and electrode, respectively. The values of R_b and R_{gb} at 25°C were 211 Ωcm^2 and 49 Ωcm^2, respectively (sample size: 13 mmϕ, 2 mm^t). The grain boundary contribution to the total resistance ($R_{gb}/(R_b + R_{gb})$) was ~20%, which is comparable to that of any other family of lithium garnet-type oxides.[7-12] The Nyquist plots of $Li_{7-X}La_3(Zr_{2-X}, Nb_X)O_{12}$ remained constant for

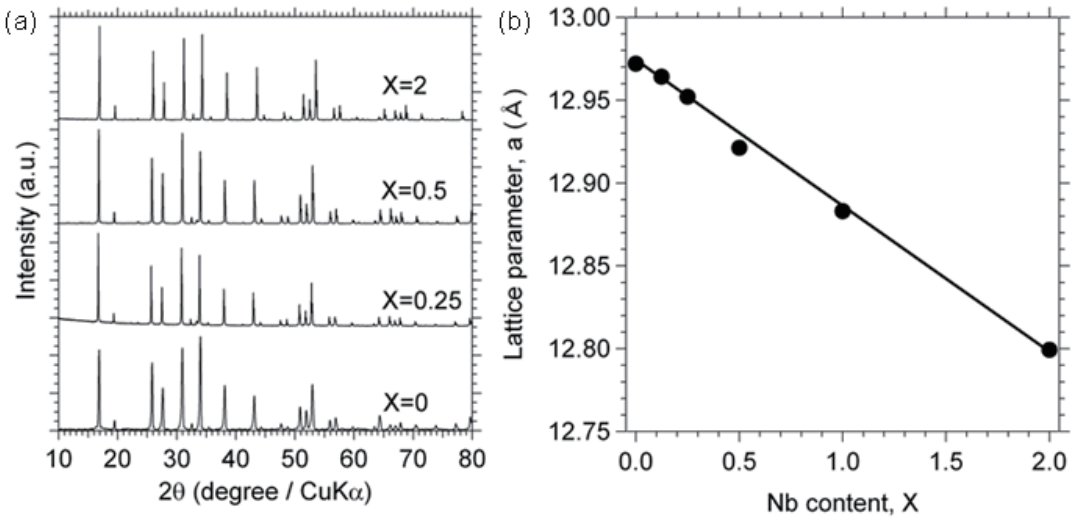

Fig. 1 (a) XRD patterns of $Li_{7-X}La_3(Zr_{2-X}, Nb_X)O_{12}$ (X = 0-2) samples. (b) Change in the lattice parameter of $Li_{7-X}La_3(Zr_{2-X}, Nb_X)O_{12}$ as a function of Nb content. The solid line is shown as a visual guide.

a week, independent of exposure time in air at room temperature, demonstrating the stability of $Li_{7-X}La_3(Zr_{2-X}, Nb_X)O_{12}$ at room temperature in air.

The temperature dependence of the total (bulk plus grain-boundary) lithium ion conductivity of $Li_{7-X}La_3(Zr_{2-X}, Nb_X)O_{12}$ is shown in **Fig. 3**(a). The lithium ion conductivity was linear and obeyed the Arrhenius law ($\sigma = A \exp(-E_a/kT)$, where A is the frequency factor, k is the Boltzmann constant, T is the absolute temperature, and E_a is the activation energy, indicating that no structure or phase changes occurred in the observed temperature range. The lithium ion conductivity at 25 °C and the activation energy are plotted in Fig. 3(b). The lithium ion conductivity increased with X, reaching a maximum of 0.8 mS cm^{-1} at X = 0.25. In contrast, the activation energy reached a minimum value of ~30 $kJmol^{-1}$ at the same value of X = 0.25. The crystal structure of lithium garnet-type oxide is shown in **Fig. 4**. Lithium ions occupy the 24 d and 96 h sites, so it is considered that the lithium ion conduction pathway exists between these sites. However, not all of the lithium ions in the crystal structure contribute to conduction. The lithium ions that occupy certain sites can only act as charge carriers when the adjacent site is vacant. Therefore, the number of the lithium ions that contribute to conduction is dependent on the occupancy and vacancy of each lithium ion site. The composition dependence of each lithium ion site in $Li_{7-X}La_3(Zr_{2-x}, Ta_X)O_{12}$ is already known.[14] The occupancies of the two lithium ion sites (24 d and 96 h) then become the same at X = 0.25. Therefore, improvement in the lithium ion conduction of $Li_7La_3Zr_2O_{12}$ by Nb substitution is expected to improve the number of conduction carriers by optimization of each of the lithium sites in lithium garnet-type oxide.

The potential window of $Li_{6.75}La_3(Zr_{1.75}, Nb_{0.25})O_{12}$ was measured using cyclic voltammetry (**Fig. 5**). Lithium deposition and dissolution peaks were observed near

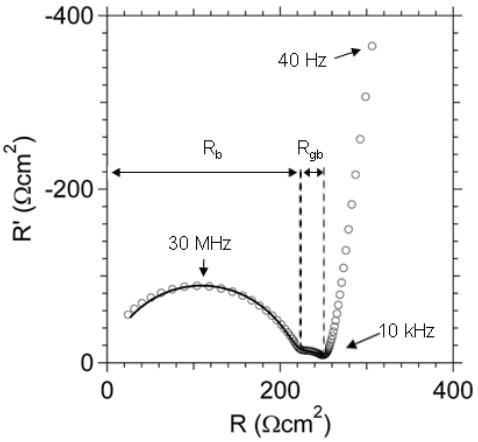

Fig. 2 Nyquist plot (40 Hz to 110 MHz) of $Li_{6.75}La_3(Zr_{1.75}, Nb_{0.25})O_{12}$ at 25°C in air using Au electrodes. The solid line represents fitted data based on an equivalent circuit model consisting of two resistances and capacitances, representing the bulk and the grain boundary.

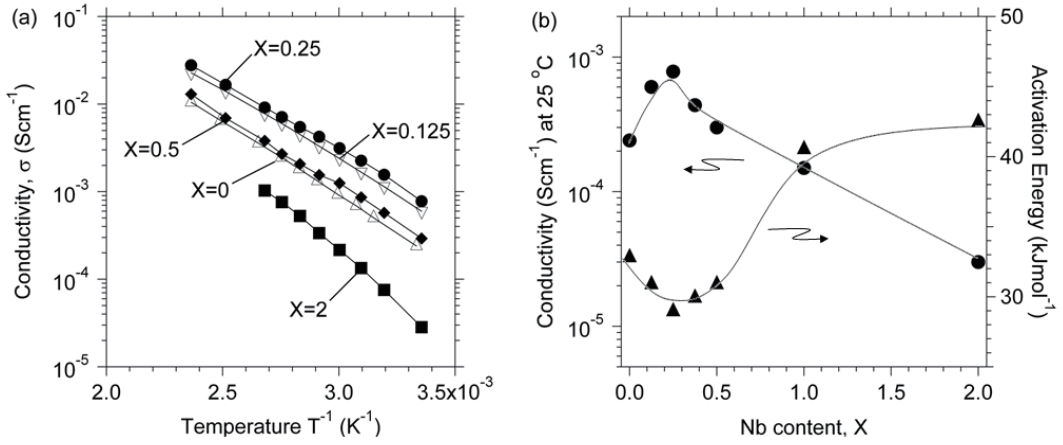

Fig. 3 (a) Temperature dependence of lithium ion conductivity of $Li_{7-X}La_3(Zr_{2-X}, Nb_X)O_{12}$ (X = 0-2) samples. (b) Lithium ion conductivity at 25°C and activation energy as a function of Nb content. The solid lines are provided as visual guides.

0 V. However, no other reactions were indicated up to 9 V, which indicates that $Li_{6.75}La_3(Zr_{1.75}, Nb_{0.25})O_{12}$ has a wide electrochemical window. Therefore, $Li_{6.75}La_3(Zr_{1.75}, Nb_{0.25})O_{12}$ is a promising solid electrolyte material for all-solid-state lithium ion batteries. An all-solid-state lithium ion battery was constructed to assess the feasibility of using $Li_{6.75}La_3(Zr_{1.75}, Nb_{0.25})O_{12}$ as a solid electrolyte material.

4. All-solid-state Lithium Ion Battery Using $Li_{6.75}La_3(Zr_{1.75}, Nb_{0.25})O_{12}$ as a Solid Electrolyte

We investigated the electrochemical performance and charge transfer resistance of an all-solid-state lithium ion battery consisting of $Li_{6.75}La_3(Zr_{1.75}, Nb_{0.25})O_{12}$ (LLZONb). The most critical parameter is the interface resistance between the electrodes and LLZONb. This is because the dominant contributor to the internal resistance of all-solid-state lithium ion batteries is not the bulk resistance of the solid electrolyte, but the interfacial resistance between the electrodes and the solid electrolyte.[15-18] In order to clarify the electrochemical performance and interfacial resistance of between cathode and Nb-doped LLZO, an all-solid-state lithium ion battery was fabricated using LLZONb (solid electrolyte), lithium (anode), and $LiCoO_2$ (LCO; cathode), which was deposited by pulsed-laser deposition (PLD). LCO was deposited by PLD (4ω-Nd:yttrium-aluminum-garnet (YAG) laser, λ = 266 nm, ~1 J cm^{-2} $pulse^{-1}$, ~20 ns, 10 Hz) on the top side of the sintered LLZONb pellet and annealing at 600 °C. The deposited thickness of the LCO film was ca. 500 nm, which was estimated from cross-sectional field emission scanning electron microscopy (FE-SEM/Hitachi S-5500) image. On the bottom of the pellet, a lithium metal foil was attached as the anode.

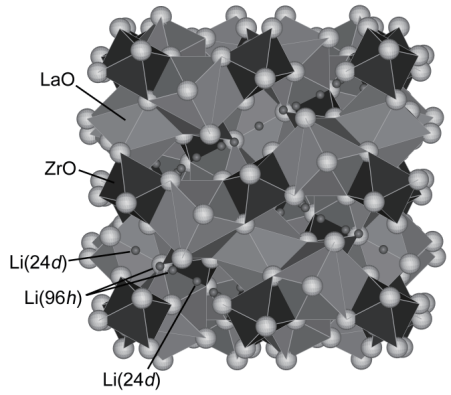

Fig. 4 Structural model of the $Li_7La_3Zr_2O_{12}$ lithium garnet-type oxide crystal.

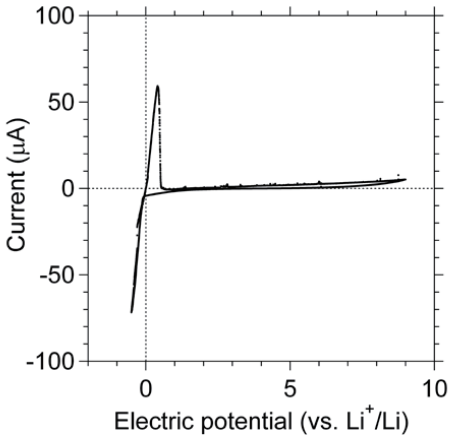

Fig. 5 A cyclic voltammogram of $Li_{6.75}La_3(Zr_{1.75}, Nb_{0.25})O_{12}$ bulk ceramic, recorded at a scanning rate of 1 mV s^{-1} at 25°C.

Figure 6 shows charge-discharge curves of the all-solid-state lithium ion battery. The plateau of the charge curve starts at approximately 3.7 V, which is slightly lower than the conventional extraction/insertion reaction of LCO (3.9 V), due to the lower crystallinity of LCO[19, 20] prepared by PLD. The theoretical electrochemical capacity of LCO is 137 mAh g^{-1}, which corresponds to 0.5 Li per CoO_2. The charge and discharge capacity at the 1st cycle were 130 and 129 mAh g^{-1}, respectively, which are approximately 90% of the theoretical capacity. The

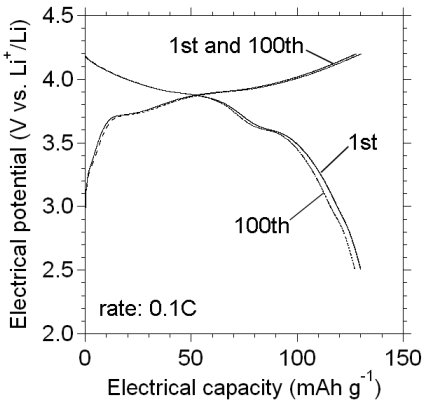

Fig. 6 Charge-discharge curves for the $LiCoO_2/Li_{6.75}La_3(Zr_{1.75}, Nb_{0.25})O_{12}/Li$ cell. The horizontal axis shows the capacity normalized by the weight of the $LiCoO_2$ cathode. Solid and dotted lines represent the 1st and 100th charge-discharge cycles, respectively.

charge-discharge curves at the 100th cycle are shown by the dotted line in Fig. 6. The charge and discharge capacity at the 100th cycle were 130 and 127 mAh g^{-1}, respectively. The retention of discharge capacity was approximately 98%, which confirms stable cycle performance for this battery.

Figure 7 shows a cross-sectional FE-SEM image of the interface between LCO and LLZONb after 100 charge-discharge cycles. No other reaction phase or exfoliation are evident at the interface. Therefore, this battery will be chemically and structurally stable during lithium intercalation–deintercalation that occurs during charging and discharging.

One of the most important parameters to improve the performance of all-solid-state lithium ion batteries is to reduce the resistivity of the interface between the cathode and the solid electrolyte. The interfacial resistance of the battery was evaluated using a two-probe AC impedance method. Measurements were conducted after charging at 3.95 V vs. Li^+/Li. A Nyquist plot for the all-solid-state lithium ion battery is shown by the open circles in **Fig. 8**(a). Three resistance components are evident, with frequencies at approximately 0.5 MHz, 100 Hz, and 1 Hz, which can be well-resolved into resistance of the LLZONb bulk (R_{LLZONb}), the interface between LCO and LLZONb ($R_{LCO/LLZONb}$), and the interface between Li and LLZONb ($R_{Li/LLZONb}$), respectively. To identify the frequency dependence of the interfacial resistance between Li and LLZONb, we constructed a Li/LLZONb/Li cell with lithium metal foils attached to both LLZONb faces. A Nyquist plot for this cell is presented in Fig. 8(b), which indicates that $R_{Li/LLZONb}$ is approximately 100 Hz. Therefore, the resistance component at approximately 1 Hz is assigned to $R_{LCO/LLZONb}$. The resistivities for R_{LLZONb}, $R_{LCO/LLZONb}$, and $R_{Li/LLZONb}$ were 120, 170, and 530 Ω cm^2, respectively. The interface resistivity between LCO and LLZONb was the same as the resistivity of the interface between LCO and LiPON prepared by physical vapor deposition.[21] A Nyquist plot for the all-solid-state lithium ion battery after 100 charge-discharge cycles is shown by the solid circles in Fig. 8(a). The interfacial resistance has not almost changed during 100 charge-discharge cycles.

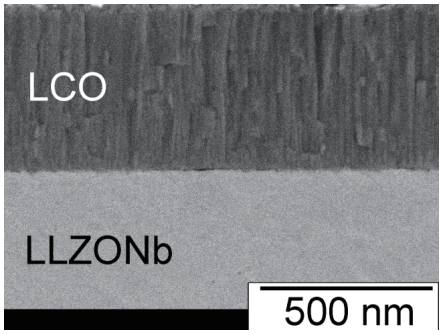

Fig. 7 Cross-sectional FE-SEM secondary electron image of the interface between $LiCoO_2$ and $Li_{6.75}La_3Zr_{1.75}Nb_{0.25}O_{12}$ after 100 charge-discharge cycles.

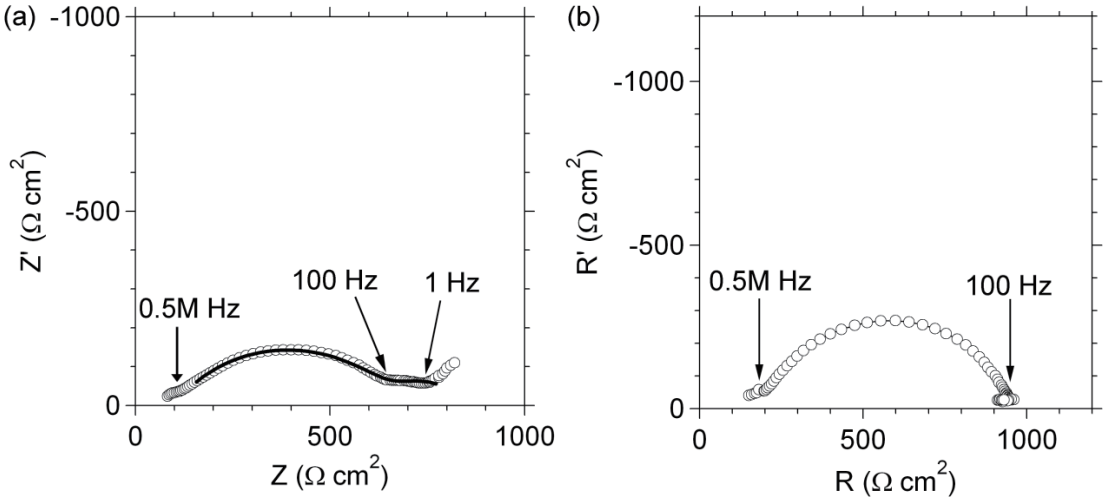

Fig. 8 (a) Nyquist plot (0.1 Hz to 1 MHz) for the $LiCoO_2/Li_{6.75}La_3(Zr_{1.75}, Nb_{0.25})O_{12}$/Li cell at 3.95 V. (b) Nyquist plot (0.1 Hz to 1 MHz) for the $Li/Li_{6.75}La_3(Zr_{1.75}, Nb_{0.25})O_{12}$/Li cell.

Therefore it is considered that interface between LCO and LLZONb has a good stable cycle performance.

Figure 9 shows an Arrhenius plot for each resistance at 3.95 V. E_a for both $R_{LCO/LLZONb}$ and $R_{Li/LLZONb}$ were ca. 30 kJ mol^{-1}, which are much lower than that for the interface between LCO and liquid organic electrolytes (ca. 60 kJ mol^{-1}).(22) The reason for this phenomenon can be understood as follows. It is considered that desolvation reaction occurs with lithium ion transfer at the interface between the electrodes and a liquid organic electrolyte. Therefore, E_a of the interfacial resistance between electrodes and liquid organic electrolytes are quite large (ca. 60 kJ mol^{-1}). However, in an all-solid-state lithium ion battery, the desolvation reaction does not occur; therefore, E_a of both $R_{LCO/LLZONb}$ and $R_{Li/LLZONb}$ would be expected to be the same as that for the LLZONb bulk electrolyte.

5 Conclusions

The lithium ion conductivity of lithium garnet-type oxide: $Li_7La_3Zr_2O_{12}$ was successfully improved by substitutional Nb-doping. The lithium ion conductivity was optimized, and reached a maximum of ~0.8 mS cm^{-1} at 12.5% niobium doping. The potential window of LLZONb showed no evidence of other reactions from 0 to 9 V. An all-solid-state lithium ion battery of LCO/LLZONb/Li was constructed. The charge and discharge capacities of this battery at the 1st cycle were 130 and 129 mAh g^{-1}, respectively, which is approximately 90% of the theoretical capacity. This battery exhibited stable cycle performance, with no other reaction phase or exfoliation at the interface after 100 charge–discharge cycles. The interfacial resistance between LCO and LLZONb at 25 °C was 170 Ω cm^2, which is comparable to that for a lithium ion battery with a liquid organic electrolyte. The activation energy of the interfacial resistance between LCO and LLZONb was lower than that for a lithium ion battery with a liquid organic electrolyte. These results indicate that LLZONb is a promising candidate as a solid electrolyte for high-power and high-capacity all-solid-state lithium ion batteries.

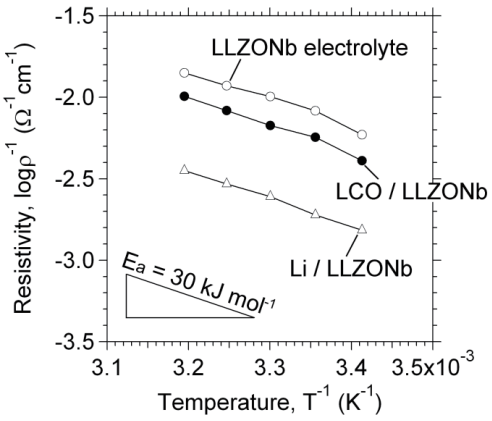

Fig. 9 Temperature dependence of the resistivity (ρ) for $Li_{6.75}La_3(Zr_{1.75}, Nb_{0.25})O_{12}$ bulk, the $LiCoO_2/Li_{6.75}La_3(Zr_{1.75}, Nb_{0.25})O_{12}$ interface and the $Li/Li_{6.75}La_3(Zr_{1.75}, Nb_{0.25})O_{12}$ interface.

References

(1) Bates, J. B., Dudeney, N. J., Gruzalski, G. R., et al., *Solid State Ionics*, Vol. 53 (1992), pp. 647-654.
(2) Hayashi, M., Takahashi, M. and Sakurai, Y., *J. Power Sources*, Vol. 174 (2007), pp. 990-995.
(3) Inaguma, Y., Liquan, C., Itoh, M., Nakamura, T., Uchida, T., Ikuta, H. and Wakihara, M., *Solid State Commun.*, Vol. 86 (1993), pp. 689-693.
(4) Kawai, H. and Kuwano, J., *J. Electrochem. Soc.*, Vol. 141 (1994), pp. L78-L79.
(5) Thangadurai, V., Shukla, A. K. and Gropalakrishnan, J., *J. Mater. Chem.*, Vol. 9 (1999), pp. 739-741.
(6) Fu, J., *Solid State Ionics*, Vol. 96 (1997), pp. 195-200.
(7) Thangadurai, V. and Weppner, W., *Advanced Functional Materials*, Vol. 15 (2005), pp. 107-112.
(8) Thangadurai, V. and Weppner, W., *J. Power Sources*, Vol. 142 (2005), pp. 339-344.
(9) Thangadurai, V. and Weppner, W., *J. Am. Ceram. Soc.*, Vol. 88 (2005), pp. 411-418.
(10) Murugan, R., Thangadurai, V. and Weppner, W., *J. Electrochem. Soc.*, Vol. 155 (2008), pp. A90-A101.
(11) Awaka, J., Kijima, N., Hayakawa, H. and Akimoto, J., *J. Solid State Chemistry*, Vol. 182 (2009), pp. 2046-2052.
(12) Murugan, R., Thangadurai, V. and Weppner, W., *Angew. Chem. Int. Ed.*, Vol. 46 (2007), pp. 7778-7781.
(13) Ohta, S., Kobayashi, T. and Asaoka, T., *J. Power Sources*, Vol. 196 (2011) pp. 3342-3345.
(14) Logéat, A., Köhler, T., Eisele, U., Stiaszny, B., Harzer, A., Tovar, M., Senyshyn, A., Ehrenberg, H. and Kozinsky, B., *Solid State Ionics*, Vol. 206 (2012), pp. 33-38.
(15) Takada, K., Inada, T., Kajiyama, A., Sasaki, H., Kondo, S., Watanabe, M., Murayama M. and Kanno, R., *Solid State Ionics*, Vol. 158 (2003), pp. 269-274.
(16) Ohta, N., Takada, K., Zhang, L.-Q., Ma, R.-Z., Osada M. and Sasaki, T., *Advanced Materials*, Vol. 18 (2006), pp. 2226-2229.
(17) Ohta, N., Takada, K., Sakaguchi, I., Zhang, L.,

Ma, R., Fukuda, K., Osada M. and Sasaki, T., *Electrochem. Commun.*, Vol. 9 (2007), pp. 1486-1490.
(18) Sakuda, A., Kitaura, H., Hayashi, A., Tadanaga, K. and Tatsumisago, M., *Electrochem. and Solid-state Letters*, Vol. 11 (2008), pp. A1-A3.
(19) Ohzuku, T. and Ueda, A., *J. Electrochem. Soc.*, Vol. 141 (1994), pp. 2972-2977.
(20) Gummow, R. J. and Thackeray, M. M., *Mat. Res. Bull.*, Vol. 27 (1992), 327-337.
(21) Iriyama, Y., Kako, T., Yada, C., Abe, T. and Ogumi, Z., *J. Power Sources*, Vol. 146 (2005) pp. 745-748.
(22) Yamada, I., Abe, T., Iriyama, Y. and Ogumi, Z., *Electrochem. Commun.*, Vol. 5 (2003), pp. 502-505.

Shingo Ohta
Research Field:
- Solid State Ionics
Academic Degree: Dr.Eng.
Academic Society:
- The Japan Society of Applied Physics

Tetsuro Kobayashi
Research Fields:
- Electrochemistry
- Battery
Academic Degree: Dr.Eng
Academic Societies:
- The Electrochemical Society of Japan
- The Solid State Ionics Society of Japan
- Ionic Liquid Research Association, Japan

Takahiko Asaoka
Research Fields:
- Electrochemistry
- Battery & Fuel Cell
Academic Societies:
- The Electrochemical Society
- The Electrochemical Society of Japan